

An improved limit on the axion-photon coupling from the CAST experiment

S Andriamonje², S Aune², D Autiero^{1‡}, K Barth¹, A Belov¹¹,
 B Beltrán^{6§}, H Bräuninger⁵, J M Carmona⁶, S Cebrián⁶,
 J I Collar⁷, T Dafni^{2,4}, M Davenport¹, L Di Lella^{1||},
 C Eleftheriadis⁸, J Englhauser^{5¶}, G Fanourakis⁹,
 E Ferrer Ribas², H Fischer¹⁰, J Franz¹⁰, P Friedrich⁵,
 T Geralis⁹, I Giomataris², S Gninenko¹¹, H Gómez⁶,
 M Hasinoff¹², F H Heinsius¹⁰, D H H Hoffmann^{3,4},
 I G Irastorza^{2,6}, J Jacoby¹³, K Jakovčić¹⁵, D Kang¹⁰,
 K Königsman¹⁰, R Kotthaus¹⁴, M Krčmar¹⁵, K Kousouris⁹,
 M Kuster^{4,5}, B Lakić¹⁵, C Lasseur¹, A Liolios⁸, A Ljubičić¹⁵,
 G Lutz¹⁴, G Luzón⁶, D Miller⁷, A Morales⁶⁺, J Morales⁶,
 A Ortiz⁶, T Papaevangelou¹, A Placci¹, G Raffelt¹⁴, H Riege⁴,
 A Rodríguez⁶, J Ruz⁶, I Savvidis⁸, Y Semertzidis^{16*},
 P Serpico¹⁷, L Stewart¹, J Vieira⁷, J Villar⁶, J Vogel¹⁰,
 L Walckiers¹ and K Zioutas^{1,16}
 (CAST Collaboration)

¹European Organization for Nuclear Research (CERN), CH-1211 Genève 23, Switzerland

²DAPNIA, Centre d'Études Nucléaires de Saclay, Gif-sur-Yvette, France

³Gesellschaft für Schwerionenforschung, GSI-Darmstadt, Plasmaphysik, Planckstr. 1, 64291 Darmstadt, Germany

⁴Technische Universität Darmstadt, Institut für Kernphysik, Schlossgartenstrasse 9, 64289 Darmstadt, Germany

⁵Max-Planck-Institut für extraterrestrische Physik, Geissenbachstrasse, 85748 Garching, Germany

⁶Instituto de Física Nuclear y Altas Energías, Universidad de Zaragoza, Zaragoza, Spain

⁷Enrico Fermi Institute and KICP, University of Chicago, Chicago, IL, USA

⁸Aristotle University of Thessaloniki, Thessaloniki, Greece

⁹National Center for Scientific Research "Demokritos", Athens, Greece

¹⁰Albert-Ludwigs-Universität Freiburg, Freiburg, Germany

¹¹Institute for Nuclear Research, Russian Academy of Sciences, Moscow, Russia

‡ Present address: Inst. de Physique Nucléaire, Lyon, France.

§ Present address: Department of Physics, Queen's University, Kingston, Ontario K7L 3N6, Canada

|| Present address: Scuola Normale Superiore, Pisa, Italy

¶ On leave

+ Deceased

* Permanent address: Brookhaven National Laboratory, NY-USA

¹²Department of Physics and Astronomy, University of British Columbia, Vancouver, Canada

¹³Johann Wolfgang Goethe-Universität, Institut für Angewandte Physik, Frankfurt am Main, Germany

¹⁴Max-Planck-Institut für Physik (Werner-Heisenberg-Institut), Föhringer Ring 6, 80805 München, Germany

¹⁵Rudjer Bošković Institute, Bijenička cesta 54, P.O.Box 180, HR-10002 Zagreb, Croatia

¹⁶University of Patras, Patras, Greece

¹⁷Particle Astrophysics Center - Fermi National Accelerator Laboratory, Batavia, IL 60510, USA

E-mail: Milica.Krcmar@irb.hr

Abstract. We have searched for solar axions or similar particles that couple to two photons by using the CERN Axion Solar Telescope (CAST) setup with improved conditions in all detectors. From the absence of excess X-rays when the magnet was pointing to the Sun, we set an upper limit on the axion-photon coupling of $g_{a\gamma} < 8.8 \times 10^{-11} \text{ GeV}^{-1}$ at 95% CL for $m_a \lesssim 0.02 \text{ eV}$. This result is the best laboratory limit over a broad range of axion masses and for $m_a \lesssim 0.02 \text{ eV}$ also supersedes the previous limit derived from energy-loss arguments on globular-cluster stars.

Keywords: axions

PACS numbers: 95.35.+d; 14.80.Mz; 07.85.Nc; 84.71.Ba

1. Introduction

The Peccei-Quinn (PQ) mechanism [1–3] remains perhaps the most compelling explanation of the CP problem of strong interactions. The existence of a new chiral $U(1)$ symmetry that is spontaneously broken at some large energy scale f_a would allow for the dynamical restoration of the CP symmetry in QCD. An inevitable consequence of this mechanism is the existence of axions, the Nambu-Goldstone bosons of $U(1)_{\text{PQ}}$ [4, 5]. Axions are pseudoscalar particles with properties closely related to those of neutral pions. In particular, their mass and interaction strengths can be obtained by a simple rescaling from the corresponding π^0 properties (see equations (3) and (4) below). Unsuccessful experimental searches [6] and astrophysical limits [7] imply that axions, if they exist, must be very light and very weakly interacting, yet they are not necessarily harmless because they are a leading candidate for the cold dark matter of the universe [8–11]. Moreover, several approaches to a unified description of dark energy and dark matter involving pseudo Nambu-Goldstone bosons have been put forward recently [12–14].

Experimental strategies to find “invisible axions” or more general “axion-like particles” (ALPs) include the cavity searches for galactic dark matter axions [15–19], searches for solar axions based on the “helioscope” method [15, 20–24], the Bragg scattering technique [25–28] or the resonant method involving nuclear couplings [29–31], the polarization of light propagating through a transverse magnetic field [32–35], and the “shining-light-through-walls” method [34, 36–44].

Almost all of these past, present or future experiments rely on the axion coupling to two photons that is described by the Lagrangian term

$$\mathcal{L}_{a\gamma} = -\frac{1}{4} g_{a\gamma} F_{\mu\nu} \tilde{F}^{\mu\nu} a = g_{a\gamma} \mathbf{E} \cdot \mathbf{B} a, \quad (1)$$

where a is the axion field, F the electromagnetic field-strength tensor, \tilde{F} its dual, \mathbf{E} the electric, and \mathbf{B} the magnetic field. The axion-photon coupling strength is quantified by

$$g_{a\gamma} = \frac{\alpha}{2\pi} \frac{1}{f_a} \left(\frac{E}{N} - \frac{2}{3} \frac{4+z+w}{1+z+w} \right), \quad (2)$$

where $z \equiv m_u/m_d$ and $w \equiv m_u/m_s \ll z$ are quark-mass ratios. The canonical values frequently used in the axion literature are $z = 0.56$ and $w = 0.028$ [45, 46], although, for example, z could lie in the range 0.3–0.6 [6]. However, by far the largest uncertainty in the relation between $g_{a\gamma}$ and f_a comes from the model-dependent ratio E/N of the electromagnetic and color anomalies of the axial current associated with the axion field. Frequently cited generic examples are the Kim-Shifman-Vainshtein-Zakharov (KSVZ) model [47, 48] where $E/N = 0$ and the Dine-Fischler-Srednicki-Zhitnitskii (DFSZ) model [49, 50] where $E/N = 8/3$, but a much broader range of possibilities exists [51]. The KSVZ model often serves as a prototype for a hadronic model where axions do not couple directly to ordinary quarks and charged leptons.

The second parameter relevant for axion searches is the axion mass, that is related to the PQ symmetry breaking scale f_a by

$$m_a = \frac{z^{1/2}}{1+z} \frac{f_\pi m_\pi}{f_a} = 6 \text{ eV} \frac{10^6 \text{ GeV}}{f_a}, \quad (3)$$

where $z = 0.56$ was assumed. Here, $m_\pi = 135 \text{ MeV}$ is the pion mass and $f_\pi \approx 92 \text{ MeV}$ is its decay constant. In terms of the axion mass, the axion-photon coupling is

$$g_{a\gamma} = \frac{\alpha}{2\pi} \left(\frac{E}{N} - \frac{2}{3} \frac{4+z}{1+z} \right) \frac{1+z}{z^{1/2}} \frac{m_a}{m_\pi f_\pi}. \quad (4)$$

This linear relationship between $g_{a\gamma}$ and m_a defines the “axion line” for a given axion model in the $g_{a\gamma}$ – m_a parameter space[‡]. Barring fine-tuned cancellations, QCD axions are expected to lie near the narrow band of parameters in the $g_{a\gamma}$ – m_a plane that is defined by the corresponding π^0 properties.

Currently, laboratory searches for axions from the Sun [21–23, 26–28] are being extended by the CERN Axion Solar Telescope (CAST). It takes advantage of the expected solar axion flux that would be produced by the Primakoff effect, i.e., the conversion of thermal photons in the Sun into axions in the presence of the electric fields of the charged particles in the solar interior. CAST itself then uses the reverse process of coherent axion-photon conversion in a “magnetic telescope,” i.e., in the bores of a 9.26 m long LHC dipole magnet oriented toward the Sun. CAST has recently reported the best laboratory limit obtained so far of $g_{a\gamma} < 1.16 \times 10^{-10} \text{ GeV}^{-1}$ for $m_a \lesssim 0.02 \text{ eV}$ [24]. This limit is comparable to the most severe constraint from the population of horizontal-branch (HB) stars in globular clusters that implies $g_{a\gamma} \lesssim 10^{-10} \text{ GeV}^{-1}$ [7, 52].

Here we report new results from the CAST experiment obtained in 2004 with improved conditions in all detectors. In addition, the solar axion flux is calculated from a modern solar model for the purpose of the CAST data interpretation. For the first time we obtained better sensitivity than that arising from energy-loss arguments on globular cluster stars.

The result reported here provides our final limit for the CAST vacuum setup (so-called CAST phase I) where the sensitivity is essentially limited to $m_a \lesssim 0.02 \text{ eV}$ as explained below. This implies that CAST has not yet reached the “axion line” in the $g_{a\gamma}$ – m_a space, but rather provides the most restrictive limits on the two-photon vertex of axion-like particles that are somewhat lighter for a given interaction strength than expected for QCD axions. Meanwhile, CAST has been refurbished as a tuning experiment, planning to explore the mass region up to about 1 eV (CAST phase II). CAST will then be the first laboratory experiment to probe QCD axion models and will also be sensitive to the existence of large extra dimensions [53], introduced in the world-brane scenarios to solve the hierarchy problem in particle physics [54].

We begin in section 2 with a new calculation of the solar axion flux. In section 3 we briefly describe the CAST experiment. In section 4 we report the 2004 measurements

[‡] Depending on the value of E/N , the axion-photon coupling can be positive or negative. In the following we always mean $|g_{a\gamma}|$ when we write $g_{a\gamma}$, i.e., we always take $g_{a\gamma}$ to be a positive number.

and their analysis. In section 5 we present the combined result of the CAST phase I and conclude in section 6.

2. Solar axion flux

2.1. General expression

Particles that interact with photons by the Lagrangian of equation (1) are produced in a hot thermal plasma by virtue of the fluctuating electric and magnetic fields, i.e., the fluctuations of $\mathbf{E} \cdot \mathbf{B}$ in the plasma act as a source for the production of axions or similar particles. Scalar particles couple to $(\mathbf{E}^2 + \mathbf{B}^2)$ instead of $\mathbf{E} \cdot \mathbf{B}$ for pseudoscalars. Hence for scalars, the fluctuations of \mathbf{E}^2 and \mathbf{B}^2 would play the analogous role. In principle, the axion emission rate for a given temperature, density and chemical composition can be calculated directly from the spectrum of $\mathbf{E} \cdot \mathbf{B}$ fluctuations as was done for a degenerate plasma in [55]. For the purpose of calculating the solar axion flux, this formalism gives the same result as the simpler approach where one calculates different “processes” contributing to the emission rate [56]. The dominant contribution derives from those fluctuations where \mathbf{E} is provided by the charged particles of the medium whereas \mathbf{B} comes from propagating thermal photons. This is the usual Primakoff process where a photon converts into an axion in the electric field of a charged particle. Of course, in a plasma the charged particles are correlated in such a way that charges are screened beyond a certain distance, an effect that is crucial to take into account. Other emission processes that are subdominant include the “electro-Primakoff-effect” where the \mathbf{B} field is provided by a moving electric charge, i.e., the axion is produced from two virtual photons, each attached to a charged particle [56]. In the Sun, all particles, including the electrons, are nonrelativistic so that the \mathbf{B} fields associated with moving electric charges are small, explaining that the electro-Primakoff effect is much less important than the ordinary Primakoff effect involving real photons.

Axions or similar particles typically will also interact with other particles in the plasma, notably the electrons and nuclei. However, in the absence of a signal it is conservative to use only those processes at the source that are implied by the very interaction structure that is used for the detection, i.e., the axion-two photon vertex. Moreover, for QCD axion models, the solar fluxes derived from other processes are expected to be much smaller than the Primakoff-induced flux if we take account of stellar energy-loss limits on these interactions. Therefore, our results are especially relevant for hadronic axions that do not couple to electrons at tree level so that the Primakoff process is expected to be the dominant process and a non-observation of axions by CAST provides new and nontrivial limits.

The transition rate for a photon of energy E into an axion of the same energy by the Primakoff effect in a stellar plasma is [57]

$$\Gamma_{\gamma \rightarrow a} = \frac{g_{a\gamma}^2 T \kappa_s^2}{32\pi} \left[\left(1 + \frac{\kappa_s^2}{4E^2} \right) \ln \left(1 + \frac{4E^2}{\kappa_s^2} \right) - 1 \right], \quad (5)$$

where T is the temperature (natural units with $\hbar = c = k_B = 1$ are used). Recoil effects are neglected so that the photon and axion energies are taken to be equal. The screening scale in the Debye-Hückel approximation is

$$\kappa_s^2 = \frac{4\pi\alpha}{T} \left(n_e + \sum_{\text{nuclei}} Z_j^2 n_j \right), \quad (6)$$

where n_e is the electron number density and n_j the number density of the j -th ion of charge Z_j .

The total axion number flux at the Earth (average solar distance D_\odot from the Earth) is

$$\Phi_a = \frac{R_\odot^3}{4\pi D_\odot^2} \int_0^1 dr \, 4\pi r^2 \int_{\omega_{\text{pl}}}^\infty dE \, \frac{4\pi k^2}{(2\pi)^3} \frac{dk}{dE} 2f_B \Gamma_{\gamma \rightarrow a}, \quad (7)$$

where $f_B = (e^{E/T} - 1)^{-1}$ is the Bose-Einstein distribution of the thermal photon bath in the solar plasma and $r = R/R_\odot$ is a dimensionless solar radial variable, normalized to the solar radius R_\odot . We take into account the plasma frequency for the photons in the system

$$\omega_{\text{pl}}^2 = \frac{4\pi\alpha n_e}{m_e}. \quad (8)$$

It enters the dispersion relation as $E^2 = k^2 + \omega_{\text{pl}}^2$ so that $dk/dE = E/k$. Of course, the value of the plasma frequency depends on the radial position in the Sun.

The approximations used in this calculation give us the axion flux for the range of X-ray energies relevant for CAST and also give us the total number flux and total energy loss rate, with an estimated precision of a few percent. However, at energies near and below a typical solar plasma frequency, i.e., for energies near or below 0.3 keV, this calculation is not appropriate because the charged particles were treated as static sources of electric fields, neglecting both recoil effects and collective motions. The charged particles of the plasma themselves undergo plasma oscillations with frequencies near ω_{pl} . Therefore, even though the thermal photon energies are cut off below ω_{pl} , the emitted axion energies can reach down to zero [57], although with a steeply falling spectrum. For applications where this low-energy flux might be of interest, perhaps the small solar axion flux at optical energies, a new calculation is needed that properly includes the dynamical aspects of the collective plasma motions, not only the static screening effects that are included here.

The X-ray telescope used in CAST is an imaging device so that we do not necessarily want to treat the Sun as a point source. We determine the differential solar axion flux as an apparent surface luminosity $\varphi_a(E, r)$ of the solar disk. Put another way, we determine the flux per unit surface area of the two-dimensional solar disk as a function of the dimensionless radial coordinate $0 \leq r \leq 1$. The total axion number flux at the Earth is

$$\Phi_a = 2\pi \int_0^1 dr \, r \int_{\omega_{\text{pl}}}^\infty dE \, \varphi_a(E, r), \quad (9)$$

i.e., φ_a is in units of $\text{cm}^{-2} \text{s}^{-1} \text{keV}^{-1}$ per unit surface area. The unit surface area is dimensionless because the radial coordinate r on the solar disk is dimensionless. Of course, instead of using a dimensionless variable r that is normalized to the solar radius, we could use one that is normalized to the apparent angular radius of the Sun in the sky. In this case, φ_a is to be multiplied with $(R_\odot/D_\odot)^2$, giving us the surface flux per steradians of solid angle and therefore the dr -integration in equation (9) would extend to the angular radius R_\odot/D_\odot of the Sun.

To determine the surface luminosity φ_a we re-write the integral over the solar volume as

$$4\pi \int_0^1 dr r^2 \rightarrow 2\pi \int_0^1 dr r \int_{\text{line of sight}} dz. \quad (10)$$

We assume the Sun to be projected on a 2-dimensional disk, i.e., we neglect parallax effects, where the ratio $R_\odot/D_\odot \approx 0.5\%$ sets the accuracy level of this approximation. We may then write the volume integral as

$$\int_{\text{line of sight}} dz = 2 \int_r^1 d\rho \frac{\rho}{\sqrt{\rho^2 - r^2}}, \quad (11)$$

where ρ is the dimensionless radial position in the Sun where the physical variables (temperature, density, etc.) have to be taken from a solar model. Altogether we find

$$\varphi_a(r, E) = \frac{R_\odot^3}{2\pi^3 D_\odot^2} \int_r^1 d\rho \frac{\rho}{\sqrt{\rho^2 - r^2}} E k f_B \Gamma_{a \rightarrow \gamma}, \quad (12)$$

where f_B and $\Gamma_{a \rightarrow \gamma}$ are to be taken at the position ρ .

2.2. Integration over solar models

In order to perform these integrations we use a recent solar model for which detailed data are publicly available, the 2004 model of Bahcall and Pinsonneault [58], which is tabulated on a fine grid (1071 points). The axion flux parameters are found to be

$$\begin{aligned} \Phi_a &= g_{10}^2 3.75 \times 10^{11} \text{ cm}^{-2} \text{ s}^{-1}, \\ L_a &= g_{10}^2 1.85 \times 10^{-3} L_\odot, \\ \langle E \rangle &= 4.20 \text{ keV}, \\ \langle E^2 \rangle &= 22.7 \text{ keV}^2, \end{aligned} \quad (13)$$

where $g_{10} = g_{a\gamma}/10^{-10} \text{ GeV}^{-1}$. The maximum of the distribution is at 3.00 keV. For self-consistency we have used the values of the solar radius ($R_\odot = 6.9598 \times 10^{10} \text{ cm}$) and of the solar luminosity ($L_\odot = 3.8418 \times 10^{33} \text{ erg s}^{-1}$) from [58].

In figure 1 we compare the differential axion flux obtained from this model with that from the 1982 model [59] that was used in an earlier calculation of the solar axion flux [20]. Even though a large number of details has changed, standard solar models and their neutrino predictions have remained remarkably robust. The same is true for the axion flux prediction that depends only mildly on the exact solar model. Even though details of our understanding of the Sun may change in the future, the solar neutrino

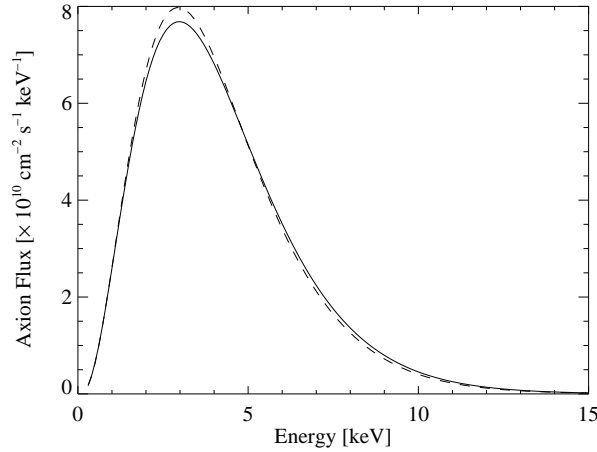


Figure 1. Comparison of the solar axion flux calculated from a modern solar model [58] (—) and an older solar model published in 1982 [59] (---). An axion-photon coupling of $1 \times 10^{-10} \text{ GeV}^{-1}$ is assumed.

measurement of all active flavors [60] has provided a direct verification of the Sun’s inner properties so that it is hard to imagine that adopting a standard solar model for the axion flux calculation could be a source of gross error.

An analytic approximation to the solar axion flux spectrum may sometimes be useful. Instead of the analytic form proposed by van Bibber et al. [20], we find that an excellent fit is provided by a three-parameter function of the kind

$$\frac{d\Phi_a}{dE} = C \left(\frac{E}{E_0} \right)^\beta e^{-(\beta+1)E/E_0}. \quad (14)$$

Here, C is a normalization constant while the fit parameter E_0 coincides with the average energy, $\langle E \rangle = E_0$. If we match the number flux, average energy, and width of the numerical spectrum with such a fit, we find (energies in keV)

$$\frac{d\Phi_a}{dE} = 6.02 \times 10^{10} \text{ cm}^{-2} \text{ s}^{-1} \text{ keV}^{-1} g_{10}^2 E^{2.481} e^{-E/1.205}. \quad (15)$$

The fit is accurate at better than about the 1% level in the interval 1 to 11 keV, while the relative accuracy is bad at very low or very high energies.

In figure 2 we show a contour plot of the solar surface luminosity in axions $\varphi_a(E, r)$ as a function of axion energy E (keV) and a dimensionless radial coordinate r on the solar disk. We also show the solar axion flux as a function of the energy for several values of r for an axion-photon coupling $g_{a\gamma} = 1 \times 10^{-10} \text{ GeV}^{-1}$. Most of the axion flux emerges from the inner 20% of the solar disk.

2.3. Do axions escape from the Sun?

CAST can detect solar axions only if these particles actually escape from the Sun after production. To estimate the axion mean free path (mfp) in the Sun we note that the photon-axion conversion rate of equation (5) is identical (in natural units) with the inverse mfp of a photon with energy E against the Primakoff process. Since we work in

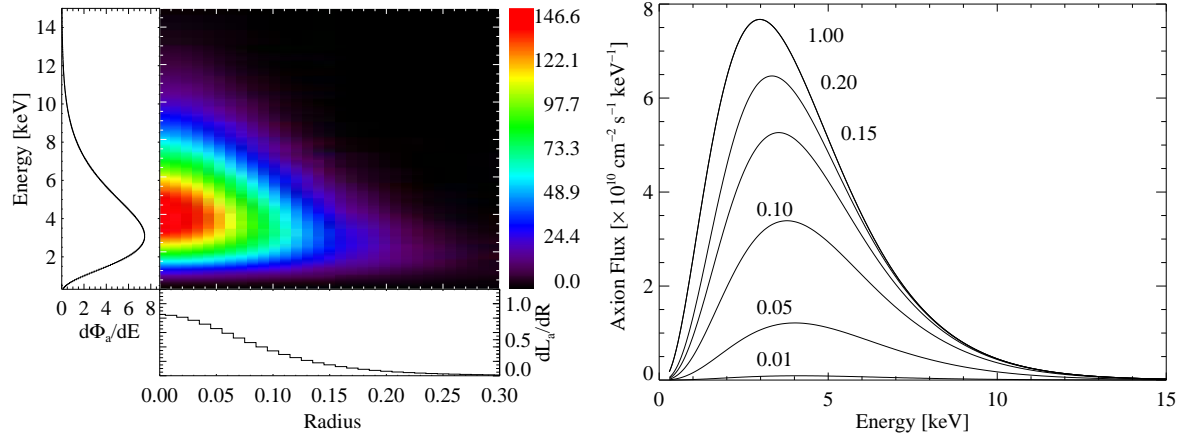


Figure 2. Left: Solar axion surface luminosity depending on energy and the radius r on the solar disk. The flux is given in units of axions $\text{cm}^{-2} \text{s}^{-1} \text{keV}^{-1}$ per unit surface area on the solar disk. Also shown is the radial distribution of the axion energy loss rate of the Sun (dL_a/dR) as well as the energy distribution of the solar axion flux ($d\Phi_a/dE$). Right: Differential solar axion spectrum, derived by integrating the model shown on the left up to different values of r in units of the solar radius R_\odot . The peak of the spectrum moves towards lower energies if integration radius moves towards the outer rim of the solar disk.

the recoil-free approximation where the energy of the photon and axion are identical, equation (5) also gives us the inverse mfp for the reverse process of an axion with energy E to be converted to a photon, i.e., of axion absorption. As an example we consider an axion with energy 4 keV, near the average of the expected spectrum, and note that the temperature at the solar center is $T \approx 1.3 \text{ keV}$ whereas the screening scale is $\kappa_s \approx 9 \text{ keV}$. The axion mfp is then found to be $\lambda_a \approx g_{10}^{-2} 6 \times 10^{24} \text{ cm} \approx g_{10}^{-2} 8 \times 10^{13} R_\odot$, or about 10^{-3} of the radius of the visible universe.

Therefore, in the absence of other interactions, the axion-photon coupling would have to be more than 10^7 times larger than the CAST limit for axions to be re-absorbed within the Sun. However, even in this extreme case axions are not harmless for the solar structure because they would then carry the bulk of the energy flux within the Sun that otherwise is carried by photons. Low-mass particles that are trapped in the Sun should interact so strongly that their mfp is smaller than that of photons [61]. Note that the photon mfp for the conditions near the solar center is less than 1 mm. Only particles with a mfp not much larger than this will leave the solar structure unaffected. They will cause a gross acceleration of the rate of energy transfer in the Sun and other stars if their mfp is much larger than this. These requirements are so extreme that for anything like axions the possibility of re-absorption is not a serious possibility. For example, if the puzzling result of the PVLAS experiment [35] is caused by low-mass particles, something must be very different about their interaction structure in that perhaps they couple very much more strongly at the optical energies tested by PVLAS than at the X-ray energies relevant in the Sun and for CAST [62] or that they are not pseudoscalars, but particles with a very different interaction structure [63]. It is impossible to discuss

such possibilities in generic terms. Rather, for a concrete model one needs to study its contribution to stellar energy loss and energy transfer.

2.4. Is the CAST limit consistent with standard solar models?

Our final limit, equation (21), on the axion-photon coupling implies that the solar axion flux is bounded by $L_a \lesssim 1.3 \times 10^{-3} L_\odot$. Self-consistent solar models including axion losses were constructed in [64]. In particular, it was found that helioseismological measurements of the sound-speed profile do not exclude $g_{a\gamma}$ much below $1 \times 10^{-9} \text{ GeV}^{-1}$ where L_a would be around $0.2 L_\odot$. It was also found that for $g_{a\gamma} = 4.5 \times 10^{-10} \text{ GeV}^{-1}$, where $L_a = 0.04 L_\odot$, the ^8B solar neutrino flux would exceed the standard prediction by about 20%. While the all-flavor ^8B flux has been measured by SNO with a precision of about 8.8% [60], the uncertainties of the flux prediction are of order 20% [65]. We conclude that the solar axion flux corresponding to the CAST limit is far below the range where it would affect helioseismology or the measured solar neutrino flux in significant ways. For the purpose of CAST it is therefore justified to treat the solar axion losses as a negligible perturbation of the standard solar models.

3. CAST experiment

A detailed description of a proposed method of detecting solar axions by the CERN Axion Solar Telescope has been given elsewhere [24, 66]. Here we only recall that CAST uses a decommissioned Large Hadron Collider (LHC) prototype magnet with a field of $B = 9.0 \text{ T}$ in the interior of two parallel pipes of length $L = 9.26 \text{ m}$ and a cross-sectional area $A = 2 \times 14.5 \text{ cm}^2$. The magnet is mounted on a moving platform with low-background X-ray detectors on either end, allowing it to track the Sun about 3 hours per day. Solar axions of a broad energy spectrum which peaks at $E \sim 4 \text{ keV}$, essentially reflecting the thermal conditions in the solar interior, may be converted into real photons inside the transverse magnetic field. The probability of this conversion in vacuum [20] is

$$P_{a \rightarrow \gamma} = \left(\frac{g_{a\gamma} B}{q} \right)^2 \sin^2 \left(\frac{qL}{2} \right), \quad (16)$$

where $q = m_a^2/2E$ is the photon-axion momentum difference. Therefore, the axion signal should appear as an excess of photons above background in three different X-ray detectors, a conventional time projection chamber (TPC), a gaseous chamber micromegas (MM), and an X-ray telescope with a charge coupled device (CCD) as focal plane detector, when the Sun and magnet are aligned. A differential flux of photons of

$$\begin{aligned} \frac{d\Phi_\gamma}{dE} &= \frac{d\Phi_a}{dE} P_{a \rightarrow \gamma} \\ &= 0.088 \text{ cm}^{-2} \text{ day}^{-1} \text{ keV}^{-1} g_{10}^4 E^{2.481} e^{-E/1.205} \left(\frac{L}{9.26 \text{ m}} \right)^2 \left(\frac{B}{9.0 \text{ T}} \right)^2 \end{aligned} \quad (17)$$

is expected at the end of the magnet in case of the coherent conversion which occurs for $qL \lesssim 1$, providing for the CAST sensitivity to the axion mass of up to 0.02 eV. Here $d\Phi_a/dE$ is the axion spectrum at the Earth, expressed by the analytic approximation (15). For $qL \gtrsim 1$ the sensitivity is reduced owing to the photon-axion momentum mismatch. To search for more massive axions, coherence can be restored by filling the magnetic conversion region with a low- Z gas whose pressure is adjusted in such a way that plasma frequency, which acts as an effective mass for the photon, equals the axion mass [20]. As one can see from equation (17), due to the $g_{a\gamma}^4$ rate suppression, a lot of effort is required to improve the existing limits on axions significantly.

4. Measurement and analysis

The new data taking has been performed after dismounting and remounting the entire setup for the X-ray detection, with some changes in the detectors, in the materials placed nearby, and in the operating conditions with respect to the data taking considered in our previous paper [24].

4.1. X-ray telescope and CCD detector

The X-ray mirror telescope is working with a CCD as the focal plane detector, placed behind one of the magnet bores at the “sunrise” end of the magnet. The sensitivity of the X-ray telescope is significantly improved compared to the 2003 data taking period by a continuous monitoring of its pointing stability, which allows us to exploit the full potential of the system. As a consequence, the area on the CCD where the axion signal is expected could be reduced by a factor of 5.8 compared to 2003. In addition, after adding new internal and external shielding components, the background level has been reduced by a factor of 1.5 in comparison with the 2003 setup. The CCD detector has shown a stable performance over the entire 2004 running period and has acquired 197 h of tracking data (when the magnet was pointing to the Sun) and 1890 h of background data (taken from the same area during the non-tracking periods). For a detailed description of the X-ray telescope design, its performance, and background systematics during the 2004 data taking period we refer to [67]. Although no significant excess signal over background could be detected with the X-ray telescope during the data taking period of 2004, a new upper limit on the axion-photon coupling could be derived. In the following sections we summarize the analysis techniques and results we obtained for the X-ray telescope.

4.1.1. Expected axion signal. As described in section 2.2 the solar axion surface luminosity $\varphi_a(E, r)$ is a function of axion energy E and the distance from the center of the solar disk r , see figure 2 and equation (12). The differential axion spectrum emitted by a circular region on the solar disk can be calculated by integrating $\varphi_a(E, r)$ from the center of the solar disk up to a radius r , resulting in spectra as shown in the right part

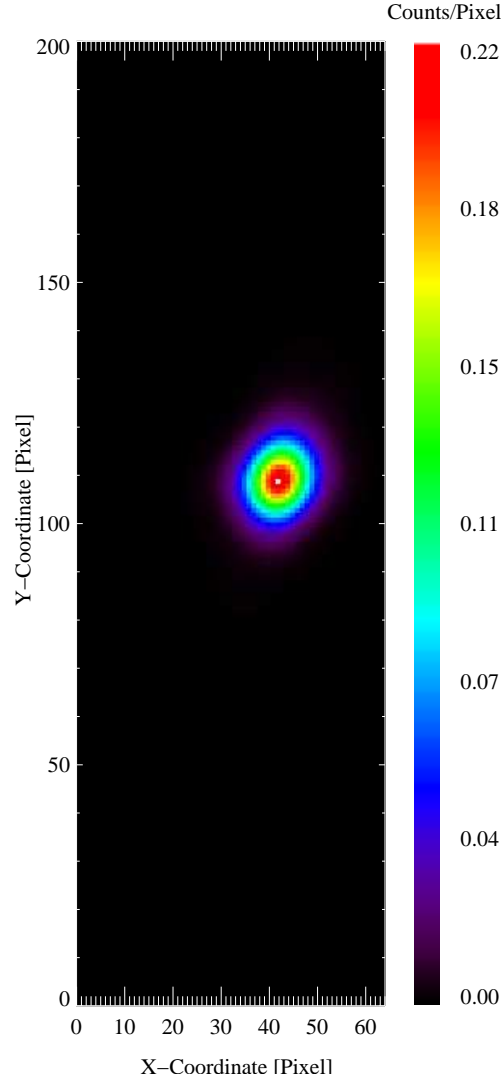


Figure 3. Expected “axion” image of the Sun as it would be observed by the CCD detector assuming the axion surface luminosity shown in figure 2 and assuming zero detector background. To determine the axion spot on the CCD, the PSF of the mirror system and the total effective area of the X-ray telescope were taken into account. The count rate integrated over the region of the spot is normalized to unity.

of figure 2. It is apparent that not only the integral flux changes, but the peak energy of the spectrum slightly shifts towards lower energies for increasing r . For $r = 1$ the spectrum peaks at lowest energies. Therefore, a photon signal resulting from axion-to-photon conversion in the magnet bore subsequently observed by the CCD would show a similar energy and radial intensity dependence, after being modified by the spatial response function of the X-ray optics (point spread function – PSF) and the energy response of the CCD detector.

To characterize the spatial intensity distribution of a potential axion signal on the CCD detector, we multiplied the axion solar surface luminosity by $P_{a \rightarrow \gamma}$ of equation (16) and folded the resulting distribution with the point spread function of the X-ray telescope. The corresponding intensity distribution (axion spot image) we would expect

on the CCD chip is shown in figure 3. The axion spot image is slightly distorted from a mere circular shape due to the PSF of the X-ray mirror optics [67]. In addition, the image is enlarged compared to an axion solar spot image multiplied with the scale factor of the mirror optics assuming a perfect linear imaging characteristics. The latter effect is a direct consequence of the finite spatial resolution of the optics, the spatial resolution of the detector (pixel size), and the limited pointing accuracy of the CAST tracking system ($\lesssim 0.01^\circ$) which spread the image of a point source. For our simulations we did not take into account that neither the PSF depends on photon energy nor the fact that it is in general a function of the position on the detector (off-axis angle). We verified that both effects are of minor importance for CAST, because the image is close to the optical axis, i.e., we have to deal with small off-axis angles, and we expect a signal in a relative narrow energy band (1–7 keV).

For a fixed m_a , the measured count-rate spectrum from axion-to-photon conversion is calculated by

$$s_i = \int_{E_i}^{E_{i+1}} dE' \int_0^\infty A(E) R(E', E) 2\pi \int_0^{r_s} \frac{d\Phi_\gamma(E, g_{a\gamma}, r)}{dE} r dr dE, \quad (18)$$

where s_i is the count rate detected in detector energy channel i in units of counts s^{-1} , $A(E)$ is the effective area of the X-ray telescope in units of cm^2 , $R(E, E')$ is the detector response function, and $d\Phi_\gamma(E, g_{a\gamma}, r)/dE$ is the differential spectrum of photons resulting from axion-to-photon conversion in the magnet for a given m_a , $g_{a\gamma}$, and the radius r in units of the solar radius R_\odot . The radius r directly corresponds to the radius of a circular signal area r_s we used to extract the potential signal, where r_s is given in detector pixel coordinates. This signal area is centered at the location where we expect the maximum signal intensity on the CCD chip. The effective area of the X-ray telescope includes the quantum efficiency of the detector, the mirror reflectivity, the influence of the finite size of the axion emission region on the Sun, and geometric effects due to, e.g., the finite diameter of the magnet bore (e.g. vignetting, see [67]).

4.1.2. Size of the signal extraction region. For a fixed location of the signal-spot on the CCD we expect that an optimum spot radius r_s exists, such that the signal-to-noise ratio of the CCD detector has a maximum. In order to find the best radius, we used the signal-to-noise ratio depending on r_s for different $g_{a\gamma}$ according to

$$\frac{S}{N}(r_s) = \frac{s(r_s, g_{a\gamma})}{\sqrt{s(r_s, g_{a\gamma}) + b(r_s)}}, \quad (19)$$

where $s(r_s, g_{a\gamma})$ is the number of counts from axion-to-photon conversion expected in the signal region for a specific $g_{a\gamma}$, calculated from equation (18) by summing over all energy bins in the 1–7 keV energy range. Further, $b(r_s)$ is the number of background counts we expect in a spot with the same area and location. To determine $b(r_s)$ we used the background data which provides enough statistics [$b(r_s) \gg 200$ counts] to avoid the optimization to be biased by low counting statistics. The background data was observed under the same axion sensitive conditions as during tracking while we were not pointing

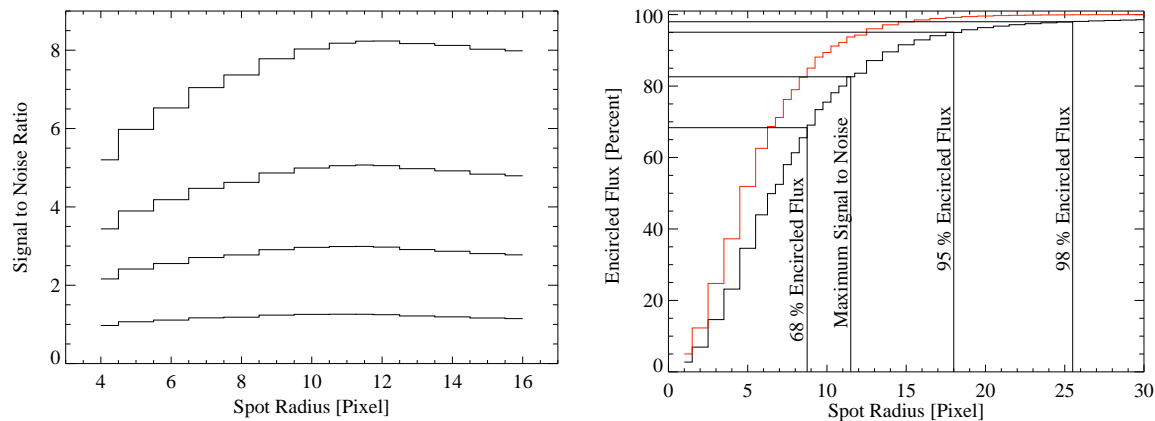


Figure 4. Left: Signal-to-noise ratio for the X-ray telescope depending on the radius of the signal-spot. The axion-photon couplings vary from $g_{a\gamma} = 2 \times 10^{-10} \text{ GeV}^{-1}$ for the lowest curve, through $g_{a\gamma} = 5, 9$ to $16 \times 10^{-10} \text{ GeV}^{-1}$ for the curve with the largest peak value. Right: The axion flux expected in the signal-spot area on the CCD relative to the axion flux for an spot radius of the size of the solar disk (encircled flux). Two cases are shown: the encircled flux for a perfect linear optics (red line) and the encircled flux for a realistic X-ray optics taking into account the point spread function of the CAST X-ray mirror system (black line).

to the Sun (see right panel of figure 5). The left panel of figure 4 shows the resulting signal-to-noise ratio depending on r_s for different values of $g_{a\gamma}$. We find a common maximum for different $g_{a\gamma}$ at a spot radius of $r_s = 11.5$ pixels which corresponds to 82.6% encircled solar axion flux (see right panel of figure 4).

4.1.3. Spectral fitting results. In order to minimize the influence of the Cu-K fluorescence line at $\approx 8 \text{ keV}$ apparent in the background spectrum of the CCD on the sensitivity of the X-ray telescope (originating in materials close to the CCD chip [67]), we restricted our analysis to the energy range from 1 to 7 keV. In total we observed 26 counts in this energy range inside the signal-spot during axion sensitive conditions (exposure time 197 h). The background is defined by the data taken from the same signal-spot area during the non-tracking periods, acquired under the same operating conditions except that the magnet was not pointing to the Sun. The spatial distribution of the observed events during tracking and non-tracking time is shown in figure 5.

The resulting low counting statistics required the use of a likelihood function in the minimization procedure to determine an upper limit on $g_{a\gamma}$, rather than a χ^2 -analysis. The likelihood function we used is based on a Poissonian p.d.f. and is given by

$$\mathcal{L}(\mu) = \prod_i^N e^{-\mu_i} \frac{\mu_i^{n_i}}{n_i!} \bigg/ \prod_i^N e^{-n_i} \frac{n_i^{n_i}}{n_i!}, \quad (20)$$

where $N = 20$ is the number of spectral bins, n_i the number of observed counts in bin i , and μ_i the value of the fit function in bin i . As a fit function $\mu_i = s_i + b_i$ was used, where b_i is the measured background and s_i the expected number of counts in the energy bin i from axion-to-photon conversion. The best estimate for $g_{a\gamma}^4$ is obtained by minimizing

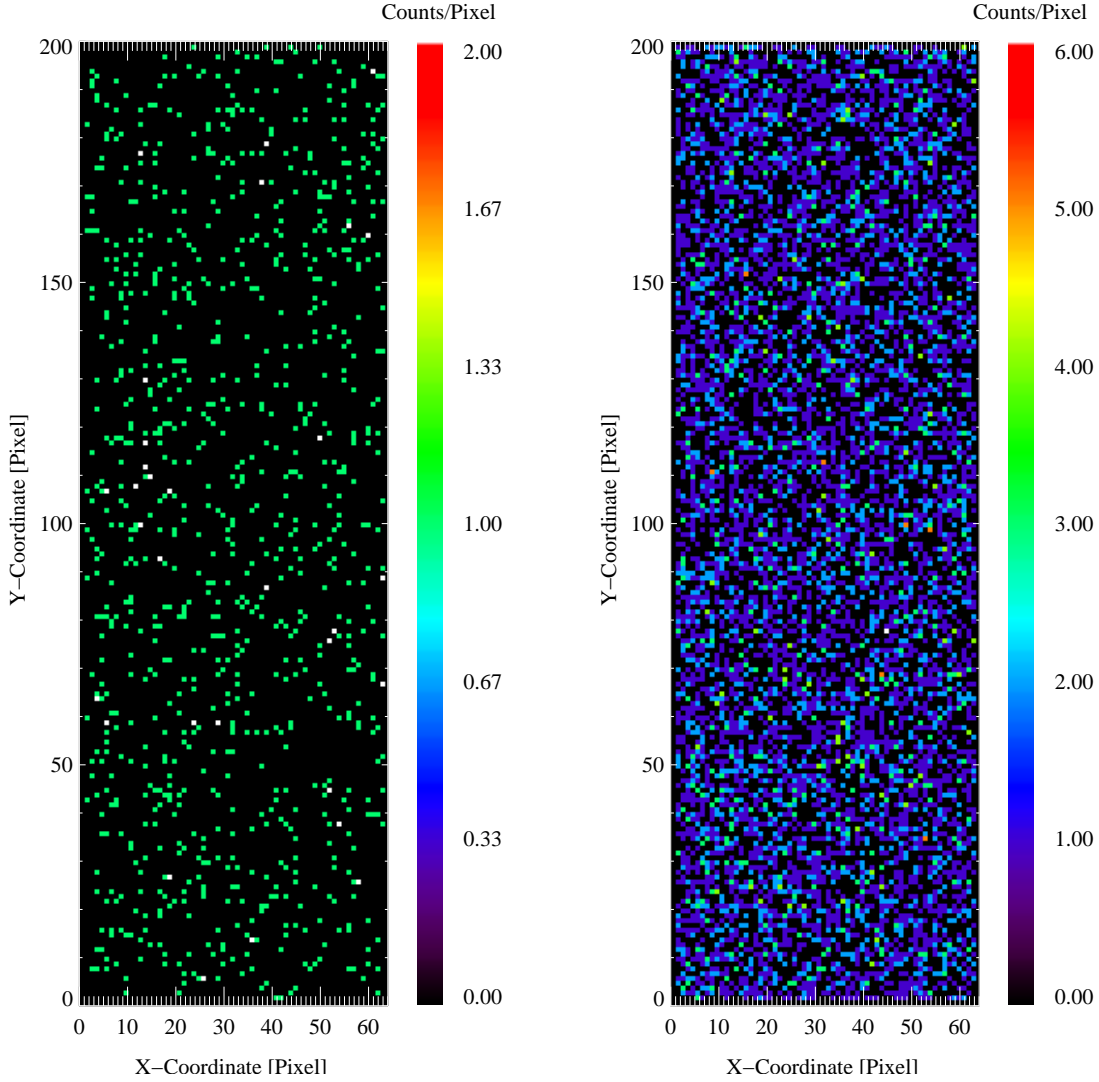


Figure 5. Left: Spatial distribution of events observed under axion sensitive conditions by the CAST X-ray telescope during the 2004 data taking period. The intensity is given in counts per pixel and is integrated over the tracking period of 197 h. Right: Background spatial distribution as observed by the CAST X-ray telescope during the 2004 data taking period. The intensity is given in counts per pixel and integrated over the full observation period of 1890 h.

$S = -2 \ln \mathcal{L}(\mu)$. In the large-sample limit the statistic S is χ^2 -distributed [6]. In the Poissonian regime, but with N relatively large, this is a reasonable assumption. The validity of the χ^2 interpretation of S in our particular case, as well as the negligible influence of the statistical uncertainty of the background on the final result have been verified with a toy Monte Carlo model. We compared the result derived with the maximum-likelihood estimator defined in equation (20) with different other maximum-likelihood techniques based on an unbinned maximum-likelihood estimator, a folded extended likelihood estimator, a binned likelihood estimator that takes into account the spectral shape of the observed background, and an extended likelihood estimator with Poissonian convolution. According to our Monte Carlo simulations all methods

are unbiased and yield identical results. We stress that in the absence of a signal (background-dominated regime), the upper limit on $g_{a\gamma}$ does not improve when taking the expected intensity distribution in the axion spot shown in figure 3 into account. This holds as long as the effective size of the signal region is kept constant.

The final analysis yields an upper limit on the axion-photon coupling of $g_{a\gamma} < 8.9 \times 10^{-11} \text{ GeV}^{-1}$ (95% CL). The observed energy spectrum together with the theoretically expected axion spectrum for the best fit value of $g_{a\gamma}$ and for the 95% CL limit on $g_{a\gamma}$ is shown in figure 6 together with the likelihood distribution of the fit. A summary of our results is given in table 1.

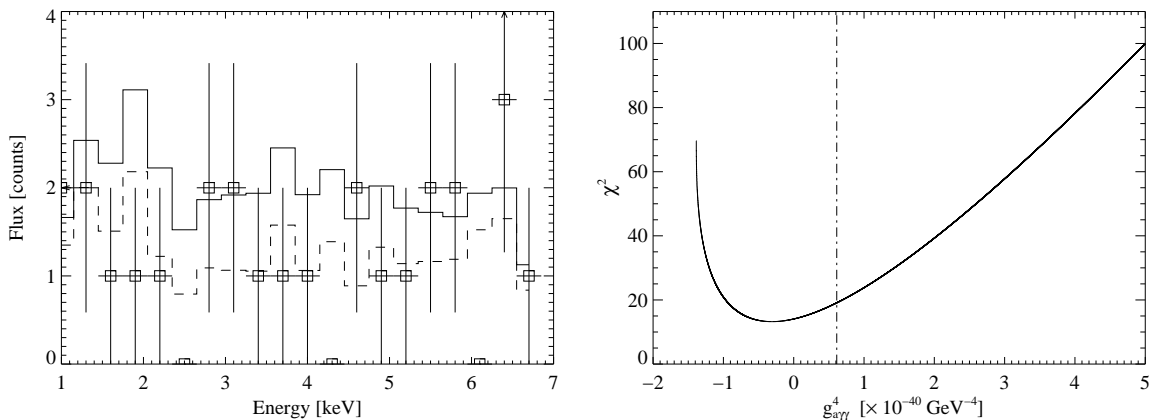


Figure 6. Left panel: Spectral distribution (\square) of the data measured with the X-ray telescope during the tracking exposure of 197 h together with the expectation μ_i for the best fit $g_{a\gamma}$ (---) and for the 95% CL limit on $g_{a\gamma}$ (—) in units of total counts per energy bin in the signal-spot area (9.35 mm^2). Right panel: Corresponding χ^2 distribution depending on $g_{a\gamma}^4$. The vertical line (— · —) marks the upper limit on $g_{a\gamma}^4$ (95% CL).

4.1.4. Systematic uncertainties. We studied the influence of systematic uncertainties on the best fit value of $g_{a\gamma}^4$ and on the upper limit on $g_{a\gamma}$. As stated in [67] statistically significant variations of the background on long (months) and short time scales (hours to days) are not apparent from the X-ray telescope data. Even if the background level would be time-dependent, it would not play a significant role, since we measure the potential signal (signal-spot) and background (area around the signal-spot) simultaneously. A crucial point in the analysis is the definition of the area where the background is taken from. Ideally, if the background is homogeneous spatially distributed, the area surrounding and close to the signal spot could be used. Since we observed no significant difference between the background level and spatial distribution during tracking and non-tracking times, we used the same signal-spot area during the non-tracking periods to define the background. Alternatively, we used tracking data and different regions on the CCD outside the signal-spot area to estimate the systematic uncertainties due to the choice of the background definition. The overall systematic

uncertainty is dominated by both the background definition and the pointing accuracy, that affects the effective area of the telescope, the location of the signal-spot and its size respectively. Other effects such as uncertainties in the detector calibration and magnet parameters are negligible. For the best fit value of $g_{a\gamma}^4$ we find

$$(g_{a\gamma}^4)_{\text{bestfit}} = (-0.31 \pm_{0.29\text{stat}}^{0.35} \pm 0.28_{\text{syst}}) \times 10^{-40} \text{ GeV}^{-4}.$$

An effect of the systematic uncertainties on the upper limit on $g_{a\gamma}$ is estimated to be less than $\sim 5\%$.

4.2. TPC and MM detector

The TPC [68], covering both bores of the “sunset” end of the magnet, was operated continuously during the entire 2004 data taking period and acquired 203 h of tracking data and 2616 h of background data. The main difference between the 2003 and 2004 experimental setup were the operation of a new differential pumping system and an improved passive shield for the detector. The purpose of the differential pumping system is to decrease the effect of gas leaks towards the magnet and to minimize the possibility of damage to the TPC windows due to sudden pressure changes or break down. As a result of the smooth operation of the TPC detector, the exposure time during 2004 was five times higher compared to 2003. The TPC is housed in a low radioactive, 5 mm thick copper box inside a low radioactive multicomponent shield (22 cm of polyethylene, 1 mm of Cd and 2.5 cm of Pb). The entire shield is permanently flushed with nitrogen, creating an over pressure which decreases the radon contamination close to the detector. The installation of the shield has reduced the TPC background level in the region between 1 and 10 keV by a factor of 4.3 compared to the background level of 2003. The typical differential counting rate in this energy interval is $4.1 \times 10^{-5} \text{ counts cm}^{-2} \text{ s}^{-1} \text{ keV}^{-1}$. One of the most important advantages of the improved background suppression is that the observed background is almost independent of the magnet pointing direction, which was not the case during the 2003 data taking period.

The micromegas detector is placed behind the other bore at the “sunrise” end of the magnet. The new MM [69] was specifically designed to eliminate the cross talk effects present at the previous detector and to improve the quality of the strips. The smooth operation of the improved MM detector during the 2004 data taking period, combined with the development of more effective off-line analysis techniques, allowed for further reduction of the background level by a factor of 2.5 compared to the 2003 running period. Due to the stability of the detector and the experiment in general, it was possible to accumulate 196 h of tracking data and 3000 h of background data. The resulting background counting rate is $5 \times 10^{-5} \text{ counts cm}^{-2} \text{ s}^{-1} \text{ keV}^{-1}$ in the 1–8.5 keV energy range.

The information of the energy scale for each detector and each run configuration is assured by periodical calibrations with the ^{55}Fe X-ray source. The hardware efficiency with respect to the photon energy has been simulated using the GEANT4 toolkit and

Table 1. 2004 data sets included in our result.

Data set	Tracking (h)	Background (h)	$(g_{a\gamma}^4)_{\text{best fit}} \pm 1\sigma_{\text{stat}}$ ($10^{-40} \text{ GeV}^{-4}$)	$\chi^2_{\text{min}}/\text{d.o.f}$	$g_{a\gamma}$ (95% CL) ($10^{-11} \text{ GeV}^{-1}$)
CCD	197	1890	$-0.31 \pm_{0.29}^{0.35}$	13.2/19	8.9
TPC	203	2616	$1.04 \pm_{1.01}^{1.02}$	17.6/17	12.9
MM	196	3000	$0.21 \pm_{1.26}^{1.27}$	24.7/14	12.7

verified by theoretical calculations and experimental data from the detectors that were characterized in the PANTER test facility in Munich [70].

4.2.1. TPC and MM data analysis and results. The results presented here were obtained after the analysis of the TPC and MM data sets listed in table 1. The analysis was performed by standard χ^2 minimization. The accumulated effective background spectrum, properly normalized, was subtracted from the corresponding tracking spectrum and the resulting data was fitted with the theoretical axion signal^{††} which scales with $g_{a\gamma}^4$ for various m_a . The obtained results are given in table 1, showing no significant excess of axion-to-photon conversion-like events. Therefore, an upper limit on $g_{a\gamma}$ at 95% confidence level was calculated for each of the data sets following the Bayesian scheme (shown in the last column of table 1). The corresponding fits are plotted in figure 7.

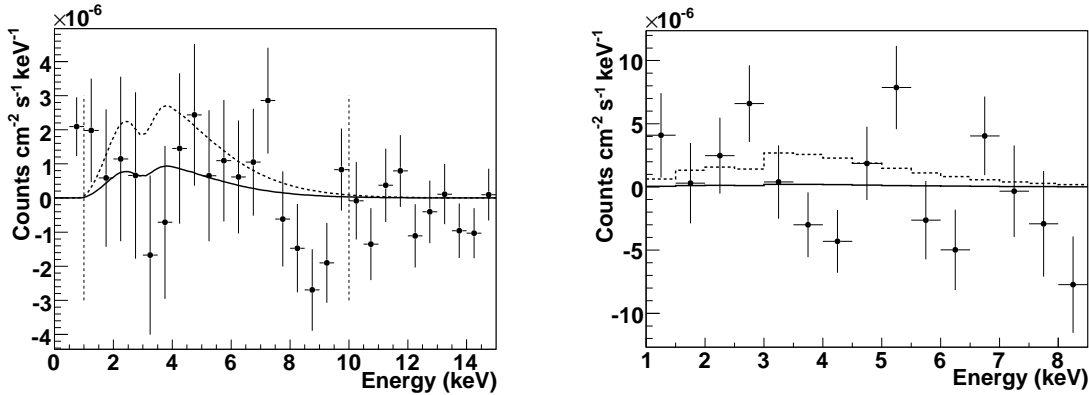


Figure 7. Panels (left) and (right) show the experimental subtracted spectrum (●) together with the expectation for the best fit $g_{a\gamma}$ (—) and for the 95% CL limit on $g_{a\gamma}$ (---) for the TPC data set and MM data set, respectively. The structure at 3 keV in the expected spectrum reflects the change in the efficiency curves of the gaseous detectors due to the Ar K-edge. The vertical dashed lines indicate the fitting window. The fully coherent conversion regime ($m_a \lesssim 0.02$ eV) is assumed.

The experimental systematic uncertainties on the present limits have been studied. The daily variation of the background caused by the environmental radon is the

^{††}The expected spectrum of axion-induced photons was calculated by equation (17) and multiplied by the detection efficiency curves.

dominant factor in the study of systematics for the MM analysis. Most of its effect is eliminated by using background data taken at times of the day as close as possible as the tracking times. The resulting upper limits for different choices of effective backgrounds clearly suggest that the systematic uncertainty is less than 2%. Systematic effects in the fitting procedure of the TPC data are considered by varying the background level until the null hypothesis test (in areas of the detector where no signal is expected) yields a result with a probability smaller than 5%. If taken as an uncertainty, this range corresponds to $\sim 10\%$ variation of the upper limit.

5. Combined result of CAST phase I data sets

The best fit values of $g_{a\gamma}^4$ obtained for each of the detector's 2004 data are reported in table 1 together with their 1σ error and the corresponding χ_{\min}^2 values and degrees of freedom. Each of the data set is individually compatible with the absence of any signal. A combined result has been obtained by multiplying the Bayesian probabilities of the three fits to get a combined probability function and obtaining the value of $g_{a\gamma}^4$ that encompasses 95% of its physically allowed (i.e. positive signals) part. The result of this operation is $g_{a\gamma} < 9.0 \times 10^{-11} \text{ GeV}^{-1}$ at 95% CL while the combination of both 2003 [24] and 2004 data gives the final limit for the CAST vacuum setup of

$$g_{a\gamma} < 8.8 \times 10^{-11} \text{ GeV}^{-1} \quad (95\% \text{ CL}). \quad (21)$$

This value is valid for $m_a \lesssim 0.02 \text{ eV}$ where the expected signal is mass independent because the axion-photon oscillation length far exceeds the length of the magnet. For higher m_a , the overall signal strength diminishes rapidly and the spectral shape differs (see equation (16)). The described procedure was repeated for different values of m_a to get the entire 95% CL exclusion line. The region excluded in the $g_{a\gamma}-m_a$ plane is shown in figure 8 together with the results of other experiments as well as astrophysical and cosmological constraints. The statistical limit on the sensitivity is mostly set by the value of $(BL)^2$ in the LHC test magnet. In general, the systematic uncertainties on the background spectrum due to its position and time dependence and due to the pointing accuracy are estimated to have an effect of less than $\sim 5\%$ in the final upper limit obtained, that is dominated by the result of the X-ray telescope.

6. Conclusion

We have searched for the coherent production of photons in a decommissioned LHC test magnet of $L = 9.26 \text{ m}$ and $B = 9 \text{ T}$, assuming the existence of an incident axion flux that is emitted from the Sun by the Primakoff process. Improvements to this experiment relative to the published 2003 results come from several changes in the detectors, in the shielding, and in the operating conditions.

In conclusion, we obtained the currently best laboratory limit on the axion-photon coupling which is by a factor 1.3 more restrictive than the CAST limit previously

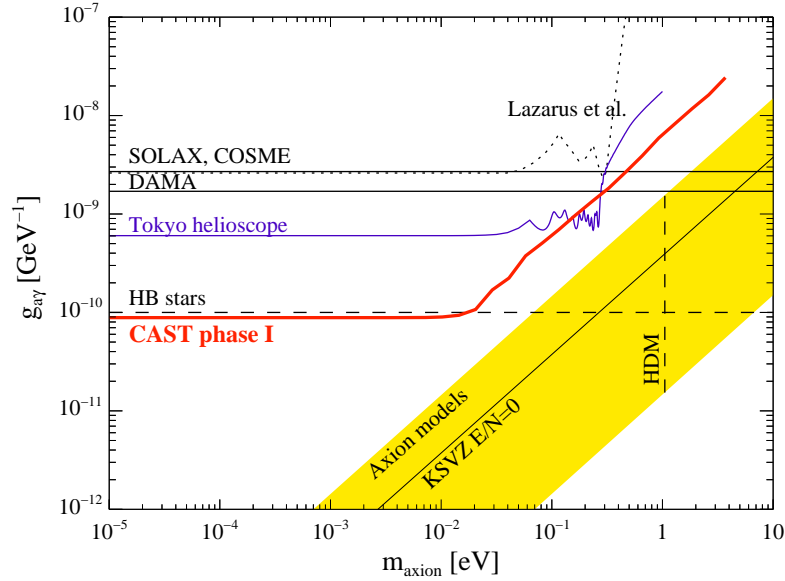


Figure 8. Exclusion plots in the axion-photon coupling versus the axion mass plane. The limit achieved by the present experiment (CAST phase I) is compared with other constraints (Lazarus et al. [21], SOLAX [26], COSME [27], DAMA [28], Tokyo helioscope [22, 23] and HB stars [7, 52]) discussed in the introduction. The vertical dashed line (HDM) is the hot dark matter limit for hadronic axions $m_a < 1.05$ eV [76] inferred from observations of the cosmological large-scale structure. The yellow band represents typical theoretical models with $|E/N - 1.95|$ in the range 0.07–7 while the black solid line corresponds to the case when $E/N = 0$ is assumed.

reported [24]. For axion masses less than 0.02 eV it supersedes the previous astrophysical limit based on the helium-burning lifetime of HB stars, as shown in figure 8. Our sensitivity does not yet touch the band of $g_{a\gamma}$ - m_a values expected for QCD axion models and thus applies to somewhat lighter axion-like particles.

Our limits can be relevant, for example, in comparison with the anomalous signature, far in excess of the QED expectation of vacuum birefringence, that has been reported by the PVLAS experiment [35]. An interpretation of this signal in terms of axion-like particles requires a coupling strength of about 10^{-5} – 10^{-6} GeV^{-1} for $m_a \sim 10^{-3}$ eV. However, this coupling is so large that the solar axion production would lead to the Sun burning out within about a 1000 years. Therefore, if the particle interpretation of PVLAS is correct, something about the underlying physics must be very different than assumed here [62, 63, 71–74]. Without a specific underlying theoretical model it is impossible to compare PVLAS and CAST in generic terms—the discrepancy is simply too large.

In order to extend our search to QCD axions, our setup has already been upgraded and the data collection has started in late 2005. The CAST experiment, being operated in a scanning mode in which the He gas pressure is varied in appropriate steps, will allow us to explore the range of possible axion masses up to about 1 eV. For the first time a laboratory experiment providing a sensitivity to $g_{a\gamma}$ of the order of that derived from HB

stars will be able to enter into the region, shown in figure 8, which is favored by axion models. In this mass range axions would provide a hot-dark matter component of the universe, similar to neutrinos [75, 76]. Another interesting feature is that in this regime of operation, when the gas is inserted in the magnet pipes, CAST could be also sensitive to the existence of (two) large extra dimensions with the compactification radius down to around 200 nm.

Acknowledgments

We thank CERN for hosting the experiment and for the contributions of J. P. Bojon, F. Cataneo, R. Campagnolo, G. Cipolla, F. Chiusano, M. Delattre, F. Formenti, M. Genet, J. N. Joux, A. Lippitsch, L. Musa, R. De Oliveira, A. Onnela, J. Pierlot, C. Rosset, H. Thiesen and B. Vullierme. We thank in particular F. James for his advice concerning the statistical treatment of the data. We acknowledge support from NSERC (Canada), MSES (Croatia) under the grant number 098-0982887-2872, CEA (France), BMBF (Germany) under the grant numbers 05 CC2EEA/9 and 05 CC1RD1/0, the Virtuelles Institut für Dunkle Materie und Neutrinos – VIDMAN (Germany), GSRT (Greece), RFFR (Russia), CICyT (Spain), NSF (USA), US Department of Energy, NASA under the grant number NAG5-10842 and the helpful discussions within the network on direct dark matter detection of the ILIAS integrating activity (Contract number: RII3-CT-2003-506222).

References

- [1] Peccei R D and Quinn H R 1977 CP Conservation in the presence of pseudoparticles *Phys. Rev. Lett.* **38** 1440
- [2] Peccei R D and Quinn H R 1977 Constraints imposed by CP conservation in the presence of pseudoparticles *Phys. Rev. D* **16** 1791
- [3] Peccei R D 2006 The strong CP problem and axions *Preprint* hep-ph/0607268
- [4] Weinberg S 1978 A new light boson? *Phys. Rev. Lett.* **40** 223
- [5] Wilczek F 1978 Problem of strong P and T invariance in the presence of instantons *Phys. Rev. Lett.* **40** 279
- [6] Yao W -M *et al* (Particle Data Group) 2006 Review of particle physics *J. Phys. G* **33** 1
- [7] Raffelt G G 2006 Astrophysical axion bounds *Preprint* hep-ph/0611350
- [8] Abbott L F and Sikivie P 1983 A cosmological bound on the invisible axion *Phys. Lett. B* **120** 133
- [9] Preskill J, Wise M B and Wilczek F 1983 Cosmology of the invisible axion *Phys. Lett. B* **120** 127
- [10] Dine M and Fischler W 1983 The not-so-harmless axion *Phys. Lett. B* **120** 137
- [11] Sikivie P 2006 Axion cosmology *Preprint* astro-ph/0610440
- [12] Kim J E and Nilles H P 2003 A quintessential axion *Phys. Lett. B* **553** 1 [hep-ph/0210402]
- [13] Mainini R and Bonometto S A 2004 Dark matter and dark energy from the solution of the strong CP problem *Phys. Rev. Lett.* **93** 121301 [astro-ph/0406114]
- [14] Takahashi F and Yanagida T T 2006 Unification of dark energy and dark matter *Phys. Lett. B* **635** 57 [hep-ph/0512296]
- [15] Sikivie P 1983 Experimental tests of the “invisible” axion *Phys. Rev. Lett.* **51** 1415
- Sikivie P 1984 (E) *Phys. Rev. Lett.* **52** 695

- [16] Bradley R *et al* 2003 Microwave cavity searches for dark-matter axions *Rev. Mod. Phys.* **75** 777
- [17] Hagmann C *et al* 1998 Results from a high-sensitivity search for cosmic axions *Phys. Rev. Lett.* **80** 2043 [astro-ph/9801286]
- [18] Asztalos S J *et al* 2004 Improved rf cavity search for halo axions *Phys. Rev. D* **69** 011101 [astro-ph/0310042]
- [19] Duffy L, Sikivie P, Tanner D B, Asztalos S, Hagmann C, Kinion D, Rosenberg L J, van Bibber K, Yu D and Bradley R F 2005 Results of a search for cold flows of dark matter axions *Phys. Rev. Lett.* **95** 091304 [astro-ph/0505237]
- [20] van Bibber K, McIntyre P M, Morris D E and Raffelt G G 1989 Design for a practical laboratory detector for solar axions *Phys. Rev. D* **39** 2089
- [21] Lazarus D M, Smith G C, Cameron R, Melissinos A C, Ruoso G, Semertzidis Y K and Nezhric F A 1992 Search for solar axions *Phys. Rev. Lett.* **69** 2333
- [22] Moriyama S, Minowa M, Namba T, Inoue Y, Takasu Y and Yamamoto A 1998 Direct search for solar axions by using strong magnetic field and x-ray detectors *Phys. Lett. B* **434** 147 [hep-ex/9805026]
- [23] Inoue Y, Namba T, Moriyama S, Minowa M, Takasu Y, Horiuchi T and Yamamoto A 2002 Search for sub-electronvolt solar axions using coherent conversion of axions into photons in magnetic field and gas helium *Phys. Lett. B* **536** 18 [astro-ph/0204388]
- [24] Zioutas K *et al* (CAST Collaboration) 2005 First results from the CERN Axion Solar Telescope *Phys. Rev. Lett.* **94** 121301 [hep-ex/0411033]
- [25] Paschos E A and Zioutas K 1994 A proposal for solar axion detection via Bragg scattering *Phys. Lett. B* **323** 367
- [26] Avignone III F T *et al* (SOLAX Collaboration) 1998 Experimental search for solar axions via coherent Primakoff conversion in a germanium spectrometer *Phys. Rev. Lett.* **81** 5068 [astro-ph/9708008]
- [27] Morales A *et al* (COSME Collaboration) 2002 Particle dark matter and solar axion searches with a small germanium detector at the Canfranc underground laboratory *Astropart. Phys.* **16** 325 [hep-ex/0101037]
- [28] Bernabei R *et al* 2001 Search for solar axions by Primakoff effect in NaI crystals *Phys. Lett. B* **515** 6
- [29] Krčmar M, Krečak Z, Stipčević M, Ljubičić A and Bradley D A 1998 Search for solar axions using ^{57}Fe *Phys. Lett. B* **442** 38 [nucl-ex/9801005]
- [30] Krčmar M, Krečak Z, Ljubičić A, Stipčević M and Bradley D A 2001 Search for solar axions using ^7Li *Phys. Rev. D* **64** 115016 [hep-ex/0104035]
- [31] Ljubičić A, Kekez D, Krečak Z and Ljubičić T 2004 Search for hadronic axions using axioelectric effect *Phys. Lett. B* **599** 143 [hep-ex/0403045]
- [32] Maiani L, Petronzio R and Zavattini E 1986 Effects of nearly massless, spin-zero particles on light propagation in a magnetic field *Phys. Lett. B* **175** 359
- [33] Raffelt G and Stodolsky L 1988 Mixing of the photon with low-mass particles *Phys. Rev. D* **37** 1237
- [34] Cameron R *et al* 1993 Search for nearly massless, weakly coupled particles by optical techniques *Phys. Rev. D* **47** 3707
- [35] Zavattini E *et al* (PVLAS Collaboration) 2006 Experimental observation of optical rotation generated in vacuum by a magnetic field *Phys. Rev. Lett.* **96** 110406 [hep-ex/0507107]
- [36] Ringwald A 2003 Production and detection of very light bosons in the HERA tunnel *Phys. Lett. B* **569** 51 [hep-ph/0306106]
- [37] Rabadan R, Ringwald A and Sigurdson K 2006 Photon regeneration from pseudoscalars at X-ray laser facilities *Phys. Rev. Lett.* **96** 110407 [hep-ph/0511103]
- [38] Kötzig U, Ringwald A and Tschentscher T 2006 Production and detection of axion-like particles at the VUV-FEL: Letter of intent *Preprint* hep-ex/0606058
- [39] Lindner A 2006 Search for axion-like particles at DESY: The ALPS project, Talk given at

- Axions at the Institute for Advanced Study* (20–22 Oct. 2006, IAS, Princeton, New Jersey), <http://www.sns.ias.edu/~axions>
- [40] Cantatore G 2006 Probing the quantum vacuum with polarized light: Results and outlook from the PVLAS experiment, Talk given at *Axions at the Institute for Advanced Study* (20–22 Oct. 2006, IAS, Princeton, New Jersey), <http://www.sns.ias.edu/~axions>
 - [41] Afanasev A V, Baker O K, McFarlane K W, Biallas G H, Boyce J R and Shinn M D 2006 Production and detection of very light spin-zero bosons at optical frequencies *Preprint* hep-ph/0605250
 - [42] Afanasev A 2006 LIPSS project: A search for photon regeneration at optical frequencies, Talk given at *Axions at the Institute for Advanced Study* (20–22 Oct. 2006, IAS, Princeton, New Jersey), <http://www.sns.ias.edu/~axions>
 - [43] Battesti R 2006 The BMV project, Talk given at *Axions at the Institute for Advanced Study* (20–22 Oct. 2006, IAS, Princeton, New Jersey), <http://www.sns.ias.edu/~axions>
 - [44] Pugnât P 2006 Laser-based experiments in high magnetic field for QED test and axion search at CERN, Talk given at *Axions at the Institute for Advanced Study* (20–22 Oct. 2006, IAS, Princeton, New Jersey), <http://www.sns.ias.edu/~axions>
 - [45] Gasser J and Leutwyler H 1982 Quark masses *Phys. Rept.* **87** 77
 - [46] Leutwyler H 1996 The ratios of the light quark masses *Phys. Lett. B* **378** 313 [hep-ph/9602366]
 - [47] Kim J E 1979 Weak interaction singlet and strong CP invariance *Phys. Rev. Lett.* **43** 103
 - [48] Shifman M A, Vainshtein A I and Zakharov V I 1980 Can confinement ensure natural CP invariance of strong interactions? *Nucl. Phys. B* **166** 493
 - [49] Dine M, Fischler W and Srednicki M 1981 A simple solution to the strong CP problem with a harmless axion *Phys. Lett. B* **104** 199
 - [50] Zhitnitskii A R 1980 *Yad. Fiz.* **31** 497
Zhitnitskii A R 1980 On possible suppression of the axion hadron interactions *Sov. J. Nucl. Phys.* **31** 260 (translation)
 - [51] Cheng S L, Geng C Q and Ni W T 1995 Axion-photon couplings in invisible axion models *Phys. Rev. D* **52** 3132 [hep-ph/9506295]
 - [52] Raffelt G G 1996 *Stars as Laboratories for Fundamental Physics* (Chicago: The University of Chicago Press)
 - [53] Horvat R, Krčmar M and Lakić B 2004 CERN Axion Solar Telescope as a probe of large extra dimensions *Phys. Rev. D* **69** 125011 [astro-ph/0312030]
 - [54] Arkani-Hamed N, Dimopoulos S and Dvali G 1998 The hierarchy problem and new dimensions at a millimeter *Phys. Lett. B* **429** 263 [hep-ph/9803315]
 - [55] Altherr T, Petitgirard E and del Río Gaztelurrutia T 1994 Axion emission from red giants and white dwarfs *Astropart. Phys.* **2** 175 [hep-ph/9310304]
 - [56] Raffelt G G 1986 Astrophysical axion bounds diminished by screening effects *Phys. Rev. D* **33** 897
 - [57] Raffelt G G 1988 Plasmon decay into low mass bosons in stars *Phys. Rev. D* **37** 1356
 - [58] Bahcall J N and Pinsonneault M H 2004 What do we (not) know theoretically about solar neutrino fluxes? *Phys. Rev. Lett.* **92** 121301 [astro-ph/0402114] see also <http://www.sns.ias.edu/~jnb/SNdata/sndata.html>
 - [59] Bahcall J N, Huebner W F, Lubow S H, Parker P D and Ulrich R K 1982 Standard solar models and the uncertainties in predicted capture rates of solar neutrinos *Rev. Mod. Phys.* **54** 767 see also <http://www.sns.ias.edu/~jnb/SNdata/sndata.html>
 - [60] Ahmed S N *et al* (SNO Collaboration) 2004 Measurement of the total active B-8 solar neutrino flux at the Sudbury Neutrino Observatory with enhanced neutral current sensitivity *Phys. Rev. Lett.* **92** 181301 [nucl-ex/0309004]
 - [61] Raffelt G G and Starkman G D 1989 Stellar energy transfer by keV-mass scalars *Phys. Rev. D* **40** 942
 - [62] Massó E and Redondo J 2005 Evading astrophysical constraints on axion-like particles *J. Cosmol.*

- Astropart. Phys.* JCAP09(2005)015 [hep-ph/0504202]
- [63] Antoniadis I, Boyarsky A and Ruchayskiy O 2006 Axion alternatives *Preprint* hep-ph/0606306
 - [64] Schlattl H, Weiss A and Raffelt G 1999 Helioseismological constraint on solar axion emission *Astropart. Phys.* **10** 353 [hep-ph/9807476]
 - [65] Bahcall J N, Serenelli A M and Basu S 2005 New solar opacities, abundances, helioseismology, and neutrino fluxes *Astrophys. J.* **621** L85 [astro-ph/0412440]
 - [66] Zioutas K *et al* 1999 A decommissioned LHC model magnet as an axion telescope *Nucl. Instrum. Methods Phys. Res. A* **425** 480 [astro-ph-9801176]
 - [67] Kuster M *et al* 2007 The X-ray telescope of CAST *New J. Phys.* submitted
 - [68] Autiero D *et al* 2007 The CAST time projection chamber *New J. Phys.* submitted
 - [69] Abbon P *et al* 2007 The micromegas detector of the CAST experiment *New J. Phys.* submitted
 - [70] Freyberg M J *et al* 2005 The MPE X-ray test facility PANTER: calibration of hard X-ray (15-50 keV) optics *Experimental Astronomy* **20** 405
 - [71] Massó E and Redondo J 2006 Compatibility of CAST search with axion-like interpretation of PVLAS results *Phys. Rev. Lett.* **97** 151802 [hep-ph/0606163]
 - [72] Mohapatra R N and Nasri S 2006 Reconciling the CAST and PVLAS results *Preprint* hep-ph/0610068
 - [73] Jäckerl J, Massó E, Redondo J, Ringwald A and Takahashi F 2006 The need for purely laboratory-based axion-like particle searches *Preprint* hep-ph/0610203
 - [74] Redondo J 2006 A model solving the PVLAS-CAST puzzle *Preprint* hep-ph/0610213
 - [75] Moroi T and Murayama H 1998 Axionic hot dark matter in the hadronic axion window *Phys. Lett. B* **440** 69 [hep-ph/9804291]
 - [76] Hannestad S, Mirizzi A and Raffelt G 2005 A new cosmological mass limit on thermal relic axions *J. Cosmol. Astropart. Phys.* JCAP07(2005)002 [hep-ph/0504059]